KI REPORTS
KIReports.org
TRANSLATIONAL RESEARCH

TRPC6-Calpain-1 Axis Promotes Tubulointerstitial Inflammation by Inhibiting Mitophagy in Diabetic Kidney Disease

Cong-Cong Liu[1,6], Jia-Ling Ji[2,6], Ze Wang[3], Xing-Jian Zhang[1], Lin Ding[4], Yao Zhang[1], Yan Zhou[5], Dong-Jie Zhang[1], Zhen-Lin Tang[1], Jing-Yuan Cao[3], Ai-Qing Zhang[2], Bi-Cheng Liu[5], Zuo-Lin Li[5] and Rui-Xia Ma[1]

[1]Department of Nephrology, Affiliated Hospital of Qingdao University, Qingdao, Shandong, China; [2]Department of Pediatrics, The Fourth Affiliated Hospital of Nanjing Medical University, Nanjing, Jiangsu, China; [3]Department of Nephrology, Nanjing University of Chinese Medicine, Nanjing, Jiangsu, China; [4]Department of Nephrology, Minda Hospital Affiliated to Hubei Minzu University, Enshi, Hubei, China; and [5]Institute of Nephrology, Zhong Da Hospital, Southeast University School of Medicine, Nanjing, Jiangsu, China

Introduction: Renal tubulointerstitial inflammation represents an effective indicator for predicting the progression of diabetic kidney disease (DKD). Mitophagy abnormality is 1 of the most important factors involved in tubule injury. However, the exact molecular mechanism underlying mitophagy abnormality-mediated tubulointerstitial inflammation in DKD remains poorly understood.

Methods: In this study, a streptozotocin-induced DKD mouse model was established and HK-2 cells treated with high glucose (HG) served as an *in vitro* model. Tubular mitophagy was regulated through pharmacological urolithin A (UA) administration. The functional effect of the transient receptor potential cation channel, subfamily C, member 6 (TRPC6) was explored using genetic interventions *in vivo* and *in vitro*.

Results: We found that renal tubulointerstitial inflammation in DKD was closely associated with mitophagy inhibition, which was mediated by disturbance of PINK1/Parkin pathway. Mitophagy activation significantly attenuated tubular injury and tubulointerstitial inflammation. Further, it was found that TRPC6 was markedly increased in DKD and played an essential role in mitophagy inhibition by activating calpain-1. Knockdown of *Trpc6* partially reversed mitophagy abnormality and consequently attenuated tubular injury and tubulointerstitial inflammation *in vivo* and *in vitro*. Finally, we found that tubular TRPC6-mediated mitophagy inhibition was blocked with BAPTA (a specific Ca^{2+} chelator) or calpeptin (a specific calpain-1 inhibitor).

Conclusion: Our study reveals that TRPC6-calpain-1 axis promotes tubulointerstitial inflammation in DKD by inhibiting mitophagy.

Kidney Int Rep (2024) **9,** 3301–3317; https://doi.org/10.1016/j.ekir.2024.08.019
KEYWORDS: calpain-1; diabetic kidney disease; mitophagy; TRPC6; tubulointerstitial inflammation

DKD, a devastating microvascular complication of diabetes mellitus, is 1 of the most common causes of end-stage renal disease. The pathogenesis of DKD is multifactorial, which is characterized by thickening of the basement membrane, podocyte injury, mesangial expansion, tubular atrophy, and interstitial inflammation and fibrosis.[1] Increasing evidence indicated that tubular injury and subsequent tubulointerstitial inflammation is 1 of the characteristic pathological features of progression of DKD.[2,3] However, the exact mechanisms underpinning tubulointerstitial inflammation in DKD require elucidation.

Packed with mitochondria and dependent on oxidative phosphorylation, the tubule epithelial cell is particularly vulnerable to injury (ischemic, hypoxic, oxidative, and metabolic),[4] contributing to tubulointerstitial inflammation. Growing evidence indicated that mitophagy, one of the most important quality

Correspondence: Rui-Xia Ma, Department of Nephrology, Affiliated Hospital of Qingdao University, Qingdao, Shandong, China. E-mail: anita1685@163.com; or Zuo-Lin Li, Institute of Nephrology, Zhong Da Hospital, Southeast University School of Medicine, Nanjing, Jiangsu, China. E-mail: zuolin_li1990@126.com

[6]C-CL and J-LJ contributed equally to this work and share first authorship.

Received 20 April 2024; revised 23 July 2024; accepted 16 August 2024; published online 23 August 2024

control mechanisms in mitochondrial homeostasis,[5] is a critical regulator of inflammation, which is a key contributor to the development and progression of DKD.[6,7] Moreover, there is a strong link between mitophagy and DKD.[8] For instance, Xiao *et al*. showed that PINK1/Parkin-mediated mitophagy was reduced in DKD.[9] Renal tubules of both humans and animals with DKD revealed accumulation of dysfunctional mitochondria, indicating inhibited or aberrant mitophagy.[10,11] However, the exact molecular mechanisms of mitophagy abnormality-mediated tubulointerstitial inflammation under the condition of DKD is unclear.

TRPC6 is a Ca^{2+}-permeable nonselective cation channel, which is widely expressed in most tissues and participates in a number of physiological processes.[12] Convincing evidence indicated that TRPC6 is responsible for the increase in intracellular Ca^{2+} levels in response to various stimuli, including components of the renin-angiotensin system and reactive oxygen species.[13] Previously, tubular TRPC6 was found to be associated with renal inflammation in DKD.[14,15] Moreover, our group demonstrated that decreasing TRPC6 expression reduces apoptosis, alleviates proteinuria, and delays the progression of renal function deterioration.[16] Recently, Salemkour *et al*.[17] reported that TRPC6 was involved in the pathogenesis of DKD through impairing autophagy. In addition, TRPC6 was observed to promote apoptosis of renal tubule epithelial cells through autophagy inhibition.[18] Therefore, we hypothesized that TRPC6 is involved in the pathogenesis of tubulointerstitial inflammation in DKD through regulating mitophagy.

METHODS

Animals

Male C57BL/6J mice (6–7 weeks old, Vital River Laboratory Animal Technology Co., Ltd., Beijing, China) were housed in an animal care facility in a temperature-controlled room (20 ± 1 °C; relative humidity 45%–65%) and had free access to food and water under a 12-hour light/dark cycle. After 12-hour of fasting, mice were intraperitoneally injected with 50 mg/kg/d of streptozotocin (Sigma-Aldrich, MO) for 5 consecutive days.[19] The control group received the same dose of citrate buffer injection. Mice with fasting blood glucose (FBG) levels above 16.7 mmol/l were considered successful diabetes models.[20] Then, the mice were randomly divided into the control group ($n = 6$), the diabetic group (DKD, $n = 6$), the diabetic group transfected with LV-*NC* (DKD + LV-*NC*, $n = 6$) or LV-*Trpc6* (DKD + LV-*Trpc6*, $n = 6$) and the diabetic group treated with gastric gavage of normal saline (DKD + Veh, $n = 6$) or UA (DKD + UA, $n = 6$).

After 4 weeks of successful modeling, gastric gavage of UA (50 mg/kg/d, MCE, NJ) for the DKD + UA group and the equal volume of normal saline (Beyotime, Shanghai, China) for the DKD + Veh group were administered once a day for 8 weeks. For lentiviral intervention, after 8 weeks of successful modeling, mice in the DKD + LV-*NC* group or the DKD + LV-*Trpc6* group were injected weekly with negative control lentivirus or *Trpc6* knockdown lentivirus (Genepharma, Shanghai, China) through the tail vein for 4 weeks. FBG was measured every 2 weeks, and body weights were measured weekly. The mice were sacrificed in week 12.

The procedures for care and use of animals were reviewed and approved by Medical Ethics Committee of Affiliated Hospital of Qingdao University (Approval number: QYFY WZLL 28182).

Cell Culture and Treatment

The human renal proximal tubular cells line (HK-2, ATCC, USA) was cultured in DMEM/F12 (Gibco, NY), containing 10% fetal bovine serum (Gibco) and 1% penicillin-streptomycin in 5% CO_2 and 95% humidity at 37 °C. The cells were divided into the normal glucose group (5.5 mM glucose), the high mannitol group (5.5 mM glucose + 29.5 mM mannitol), the HG group (35 mM glucose), the HG + si-*Trpc6* group (35 mM glucose + 50 nM *Trpc6* siRNA, Genepharma), the HG + si-*NC* group (35 mM glucose + 50 nM negative control siRNA, Genepharma), the HG + UA group (35 mM glucose + 20 μM UA, HY-100599, MCE), the HG + BAPTA group (35 mM glucose + 10 μM BAPTA, HY-100168, MCE), and the HG + calpeptin group (35 mM glucose + 1 μM calpeptin, HY-100223, MCE). The HG + DMSO groups (35 mM glucose + equal volume of DMSO, ST038, Beyotime, China) were used as control groups. After treatment of 48 hours, the cells were collected, and molecular biological experiments were performed.

Biochemical Assays

Serum creatinine, urinary creatinine, and blood urea nitrogen were measured according to instructions of commercial assay kits (Jiancheng, Nanjing, China). Urinary microalbumin level was measured using a mouse microalbuminuria enzyme-linked immunosorbent assay kit (Elabscience, Wuhan, China).

Periodic acid-Schiff and Masson's Trichrome Staining

The renal specimens were fixed with paraformaldehyde and embedded in paraffin. Using standardized protocols, Periodic acid-Schiff staining and Masson's trichrome staining were performed to assess the histologic

features. Histological images were visualized using an inverted microscope. The tubular injury was scored semi quantitatively by an observer in a blinded manner. Images of at least 20 cortical fields of Periodic acid-Schiff-stained sections were examined for each group. Tubular injury score was defined as follows: score 0: no tubular injury; score 1: <10% of tubules injured (tubular dilation, tubular atrophy, tubular cast formation, sloughing of tubular epithelial cells or loss of the brush border, and thickening of the tubular basement membrane); score 2: 10% to 25% of tubules injured; score 3: 25% to 50% of tubules injured; score 4: 50% to 74% of tubules injured; score 5: >75% of tubules injured.[21] To assess tubulointerstitial fibrosis, the area of fibrosis in Masson's trichrome-stained sections were measured using Image J software. Images of at least 20 randomly selected cortical fields for each group were evaluated blindly by an observer.

Transmission Electron Microscopy

Kidney tissues were fixed with 2.5% glutaraldehyde to observe mitophagosomes. The samples were immersed in 1% osmium tetroxide and then dehydrated with different acetone concentrations. Ultrathin sections (50–70 nm) were made after embedding. They were then stained with uranyl acetate and lead citrate. Finally, they were observed by transmission electron microscopy at 80 kV.

Mitochondrial Isolation

Mitochondria were isolated from HK-2 cells and renal cortex by using cell mitochondria isolation kit (C3601, Beyotime) and tissue mitochondria isolation kit (C3606, Beyotime), respectively.

Western Blotting

Kidney cortex sample, the cells, and isolated mitochondria were lysed in RIPA lysis buffer (Servicebio, Wuhan, China), and protein concentration was measured using a bicinchoninic acid assay (Beyotime). Equal concentrations and volumes of protein were loaded using sodium dodecyl sulfate-polyacrylamide gel electrophoresis and transferred to polyvinylidene fluoride membranes (Millipore, MA). The membranes were then blocked in NcmBlot blocking buffer (NCM Biotech, Suzhou, China) for 20 minutes and incubated overnight at 4 °C with primary antibodies against TRPC6 (1:1000, 18236-1-AP, Proteintech, IL), KIM-1 (1:1000, MA5-28211, Thermo Fisher Scentific, MA), calpain-1 (1:1000, 10538-1-AP, Proteintech), β-actin (1:10,000, AB2001, Abways, Shanghai, China), LC3B (1:1000, E5Q2K, CST, MA), P62 (1:1000, WH0008878M1, Sigma-Aldrich), PINK1 (1:1000, 23274-1-AP, Proteintech), Parkin (1:1000, sc-32282, Santa Cruz, TX) and COX IV (1:5000, 11242-1-AP, Proteintech). After incubation with horseradish peroxidase-conjugated goat antimouse or antirabbit IgG (1:3000, CST) for 1 hour at room temperature, the blots were detected with the chemiluminescence advanced system (GE Healthcare, USA).

Table 1. The primer sequences

Species	Gene	Forward primer (5′–3′)	Reverse primer (5′–3′)
Mus	*Trpc6*	GGCGGCTCTCTAAAGGCTG	TGGGGTAGTAGCCATACGGTG
Mus	*Il-1β*	GAAATGCCACCTTTTGACAGTG	TGGATGCTCTCATCAGGACAG
Mus	*Il-6*	CTGCAAGAGACTTCCATCCAG	AGTGGTATAGACAGGTCTGTTGG
Mus	*Mcp-1*	TAAAAACCTGGATCGGAACCAAA	GCATTAGCTTCAGATTTACGGGT
Mus	*Tnf-α*	CTGAACTTCGGGGTGATCGG	GGCTTGTCACTCGAATTTTGAGA
Mus	*β-actin*	GGCTGTATTCCCCTCCATCG	CCAGTTGGTAACAATGCCATGT
Homo	*Il-1β*	ATGATGGCTTATTACAGTGGCAA	GTCGGAGATTCGTAGCTGGA
Homo	*Il-6*	ACTCACCTCTTCAGAACGAATTG	CCATCTTTGGAAGGTTCAGGTTG
Homo	*Mcp-1*	CAGCCAGATGCAATCAATGCC	TGGAATCCTGAACCCACTTCT
Homo	*Tnf-α*	GAGGCCAAGCCCTGGTATG	CGGGCCGATTGATCTCAGC
Homo	*β-actin*	GGACCTGACCTGCCGTCTAG	GTAGCCCAGGATGCCCTTGA

Homo, homo sapiens; Mus, mus musculus.

mRNA Isolation and Real-Time Polymerase Chain Reaction

Total RNA from the kidney tissue and HK-2 cells were extracted using TriZol reagent (Vazyme, Nanjing, China), and mRNA was reverse transcribed using HiScript III RT SuperMix (Vazyme). Polymerase chain reaction was conducted using a 7300 real-time polymerase chain reaction detection system (Applied Biosystems, USA) with ChamQ Universal SYBR qPCR Master Mix (Vazyme). The data were normalized to the expression of β-actin, and the relative expression of the target genes was calculated using the $2^{-\Delta\Delta CT}$ method. The gene primer sequences are shown in Table 1.

Immunohistochemical and Immunofluorescence Staining

For immunohistochemical staining, paraffin sections were incubated with primary antibodies against F4/80 (1:200, ab300421, Abcam, Cambridge, UK), TRPC6 (1:200, 18236-1-AP, Proteintech), PINK1 (1:200, 23274-1-AP, Proteintech) and Parkin (1:200, sc-32282, Santa Cruz) overnight at 4 °C and subsequently analyzed with a streptavidin peroxidase detection system (Maixin Technology Co., Ltd., Fuzhou, China) according to the manufacturer's protocols.

For immunofluorescence analysis, HK-2 cells were incubated with primary antibodies against calpain-1 (1:200, 10538-1-AP, Proteintech), LC3B (1:200, E5Q2K, CST) and COX IV (1:200, 11242-1-AP, Proteintech), followed by incubation with secondary antibodies (1:1 000, ab150114 and ab150077, Abcam). Nuclei were stained with 4,6-diamidino-2-phenylindole (DAPI, Beyotime) for localization. Finally, the cells were

observed using confocal microscopy. Image analysis and quantification were performed using Image J.

Detection of Intracellular Ca^{2+} Concentration

Fluo-4 AM (S1060, Beyotime) was diluted to 3 μM working solution with PBS. For the cultured cells to be examined, the culture medium was removed and washed 3 times with PBS. Add Fluo-4 AM working solution, and the amount of solution should be sufficient to cover the cells. Fluorescent probe loading was performed by incubation at 37 °C for 30 minutes. The cells were then washed 3 times with PBS and incubated for another 20 minutes to ensure that Fluo-4 AM was completely converted to Fluo-4. Fluo-4 fluorescence at 10 seconds was detected by confocal microscopy to determine the changes in intracellular Ca^{2+} concentration. Image analysis and quantification were performed using Image J.

Statistical Analysis

Data were expressed as the mean ± SEM. All analyses were conducted using GraphPad Prism 8.0. Two groups of data were compared using the 2-tailed *t* test, and data from more than 2 groups were compared using a 1-way analysis of variance. Differences where $P < 0.05$ were considered significant.

RESULTS

Renal Tubular Injury and Tubulointerstitial Inflammation Were Observed in DKD

First, the DKD mice model was successfully established, as evidenced by elevated FBG and urinary albumin-to-creatinine ratio at week 8 and 12 (Figure 1a and b). Kidney weight-to-body weight ratio and blood urea nitrogen in DKD mice were also markedly elevated (Figure 1c and d). Histologically, loss of the brush border, tubular atrophy, and sloughing of tubular epithelial cells in DKD mice were observed (Figure 1e). Meanwhile, the expression of KIM-1 was increased in DKD mice (Figure 1f). Further, Masson's trichrome staining revealed significant tubulointerstitial fibrosis in DKD mice (Figure 1g). We found that F4/80-positive cells, indicating macrophages infiltration, were significantly increased in DKD mice (Figure 1h). Concomitantly, there were significant increases in mRNA expression levels of renal inflammatory cytokines (including *interleukin-1β*, *interleukin-6*, *monocyte chemoattractant protein-1*, and *tumor necrosis factor-α*) in DKD mice and HG-stimulated HK-2 cells, respectively (Figure 1i and j). These findings indicated that renal tubular injury and tubulointerstitial inflammation were important features of DKD.

Mitophagy Inhibition was Associated With Tubulointerstitial Inflammation in DKD

Then, mitophagosomes in renal tubular cells were imaged using transmission electron microscopy. Compared with the control group, we found that the quantity of mitophagosomes in renal tubular cells of DKD mice was significantly decreased (Figure 2a). Immunohistochemical staining indicated that PINK1 and Parkin expressions were markedly reduced in DKD mice (Figure 2b and c). Meanwhile, the expressions of LC3B-II/LC3B-I, PINK1, and Parkin protein were decreased, whereas P62 expression was increased in DKD mice and HG-stimulated HK-2 cells (Figure 2d and e). Further, colocalization of LC3B (a marker of autophagy) with COX IV (a mitochondrial marker) was decreased in HG-stimulated HK-2 cells (Figure 2f), implying that mitophagy was restrained. These data suggested that mitophagy inhibition was involved in the tubulointerstitial inflammation in DKD.

Mitophagy Activation Attenuated Renal Tubular Injury and Tubulointerstitial Inflammation in DKD

To investigate the functional effect of mitophagy on tubulointerstitial inflammation in DKD, UA, a mitophagy activator, was used *in vivo* and *in vitro*. Compared with DKD mice with normal saline administration, the number of mitophagosomes in renal tubular cells of DKD mice with UA treatment was markedly increased (Figure 3a). Immunohistochemical staining indicated that PINK1 and Parkin expression were markedly increased (Figure 3b and c). Meanwhile, the expression of LC3B-II/LC3B-I, PINK1, and Parkin were increased, whereas P62 expression was decreased with UA treatment in DKD mice and HG-stimulated HK-2 cells (Figure 3d and e). Colocalization of LC3B with COX IV was increased with UA treatment (Figure 3f). The above results revealed that mitophagy was significantly activated by UA.

We found that there were no differences in FBG levels and kidney weight-to-body weight ratio in DKD mice with normal saline or UA administration (Figure 3g and h). However, urinary albumin-to-creatinine ratio and blood urea nitrogen with UA administration were significantly reduced (Figure 3i and j). Loss of the brush border, renal tubular atrophy, sloughing of tubular epithelial cells, and the expression of KIM-1 were significantly attenuated in DKD + UA group (Figure 3k and l). Concomitantly, tubulointerstitial fibrosis was attenuated (Figure 3m). The tubulointerstitial inflammation was markedly ameliorated, evidenced by F4/80 immunohistochemical staining and mRNA expression levels of renal inflammatory cytokines (Figure 3n and o). The same pattern was found in

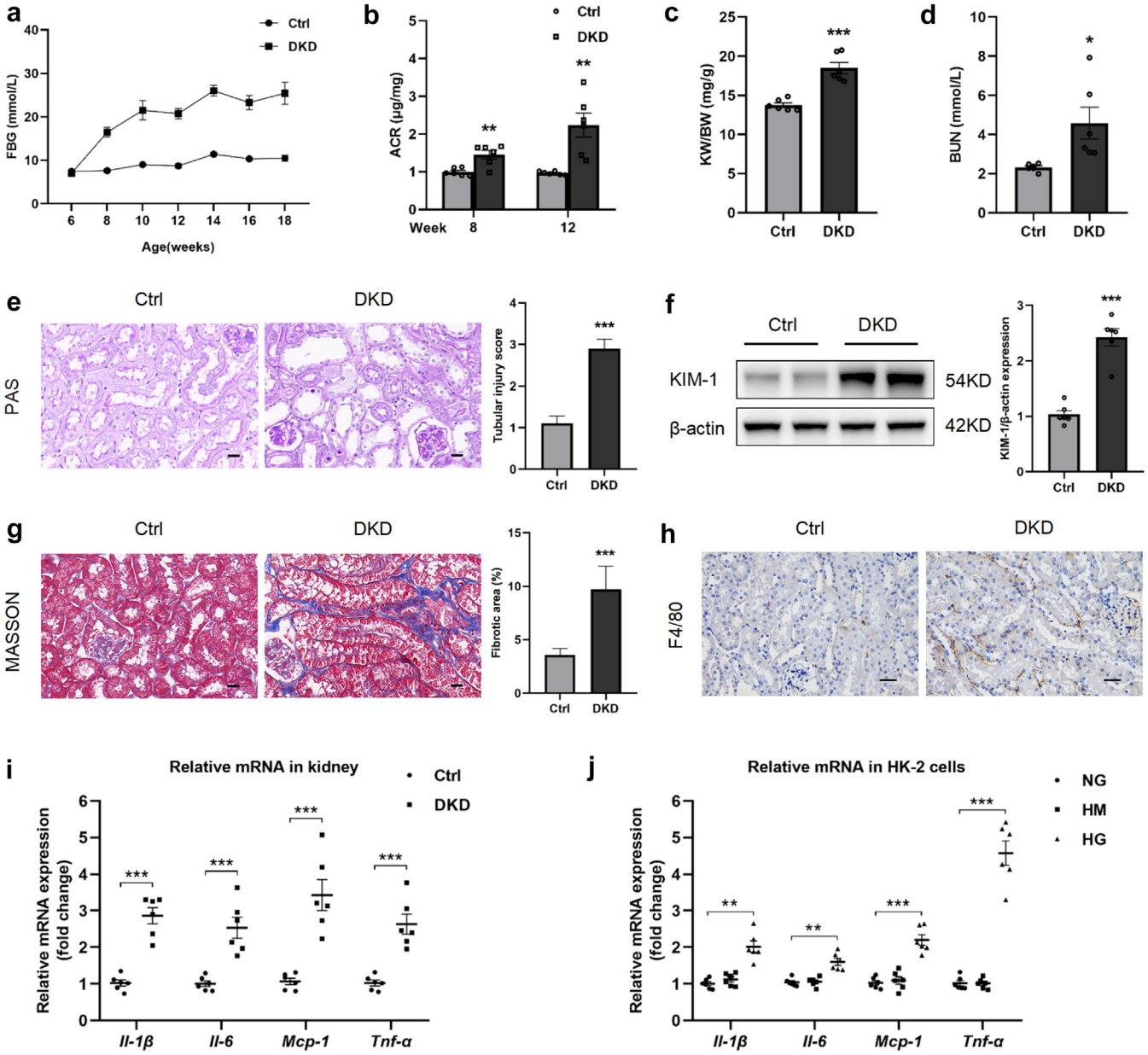

Figure 1. Renal tubular injury and tubulointerstitial inflammation were observed in DKD. (a) The levels of fasting blood glucose (FBG). (b) Urinary ACR at week 8 and week 12 after successful construction of DKD mice. (c) Kidney weight-to-body weight ratio (KW/BW). (d) The blood urea nitrogen (BUN) levels. (e) Representative images of Periodic acid-Schiff (PAS) staining of kidney sections. Scale bars, 20 μm. (f) Representative western blotting images and densitometric analysis of KIM-1 in kidney. (g) Representative images of Masson's trichrome staining and the quantitative analysis of fibrotic area. Scale bar, 20 μm. (h) Representative images of F4/80 immunohistochemical staining. Scale bars, 20 μm. (i) Real-time polymerase chain reaction analysis of the mRNA expression levels of *Il-1β*, *Il-6*, *Mcp-1*, and *Tnf-α* in kidney. (j) Real-time polymerase chain reaction analysis of the mRNA expression levels of *Il-1β*, *Il-6*, *Mcp-1* and *Tnf-α* in HK-2 cells. All data are represented as means ± SEM. $n = 6$, $^{*}P < 0.05$, $^{**}P < 0.01$, $^{***}P < 0.001$. ACR, albumin-to-creatinine ratio; Ctrl, control; DKD, diabetic kidney disease; IL, interleukin; MCP-1, monocyte chemoattractant protein-1; TNF-α, tumor necrosis factor-α.

HG-stimulated HK-2 cells with UA treatment (Figure 3p). These findings indicate that mitophagy activation attenuated renal tubular injury and tubulointerstitial inflammation in DKD.

TRPC6-Inhibited Mitophagy in DKD

Western blotting based analysis validated the upregulation of TRPC6 in DKD mice and HG-stimulated HK-2 cells (Figure 4a and b). To explore the potential effect of TRPC6 on mitophagy, TRPC6 was regulated using genetic interventions. TRPC6 was downregulated after 4 weeks of *Trpc6* knockdown lentiviral injection (Figure 4c and Supplementary Figure S1). Similar results were observed *in vitro* (Figure 4d). These data revealed that the *Trpc6* knockdown model was successfully established. Immunohistochemical staining

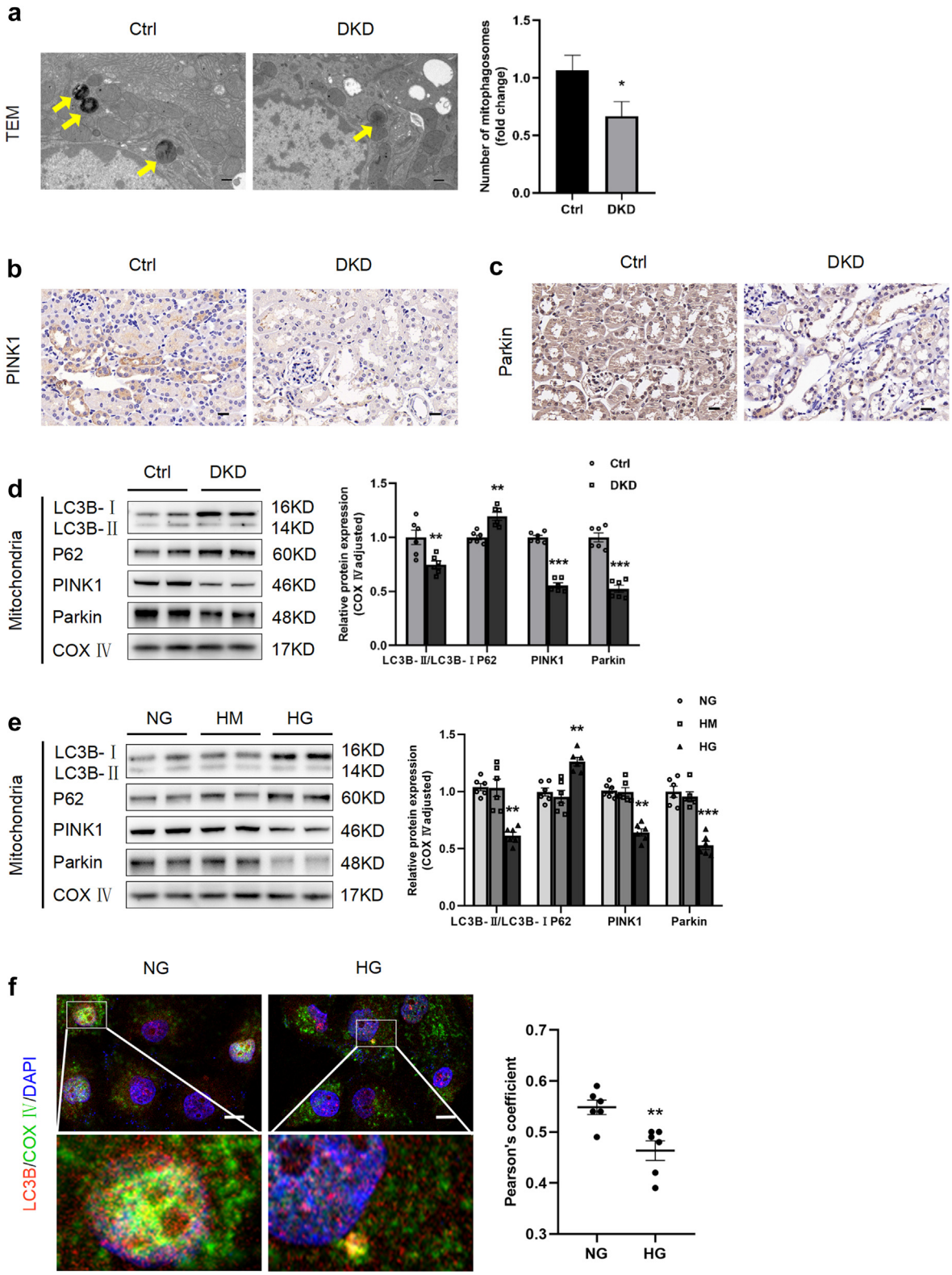

Figure 2. Mitophagy inhibition was associated with tubulointerstitial inflammation in DKD. (a) Representative transmission electron microscopy (TEM) images of intracellular mitophagosomes (arrows) in renal tubular epithelial cells from the 2 groups of mice. Scale bars, 400 nm. (b) Representative images of PINK1 immunohistochemical staining. Scale bars, 20 μm. (c) Representative images of Parkin immunohistochemical staining. Scale bars, 20 μm. (d) Representative western blotting images and densitometric analysis of LC3B, P62, PINK1, and Parkin in kidney. (e) Representative western blotting images and densitometric analysis of LC3B, P62, PINK1, and Parkin in HK-2 cells. (f) Representative confocal microscopic images and the Pearson correlation coefficient showing the colocalization of LC3B and COX IV in HK-2 cells. Nuclei were revealed using 4′,6-diamidino-2-phenylindole (DAPI) staining. Scale bars, 10 μm. All data are represented as means ± SEM. $n = 6$, $^{*}P < 0.05$, $^{**}P < 0.01$, $^{***}P < 0.001$. DKD, diabetic kidney disease.

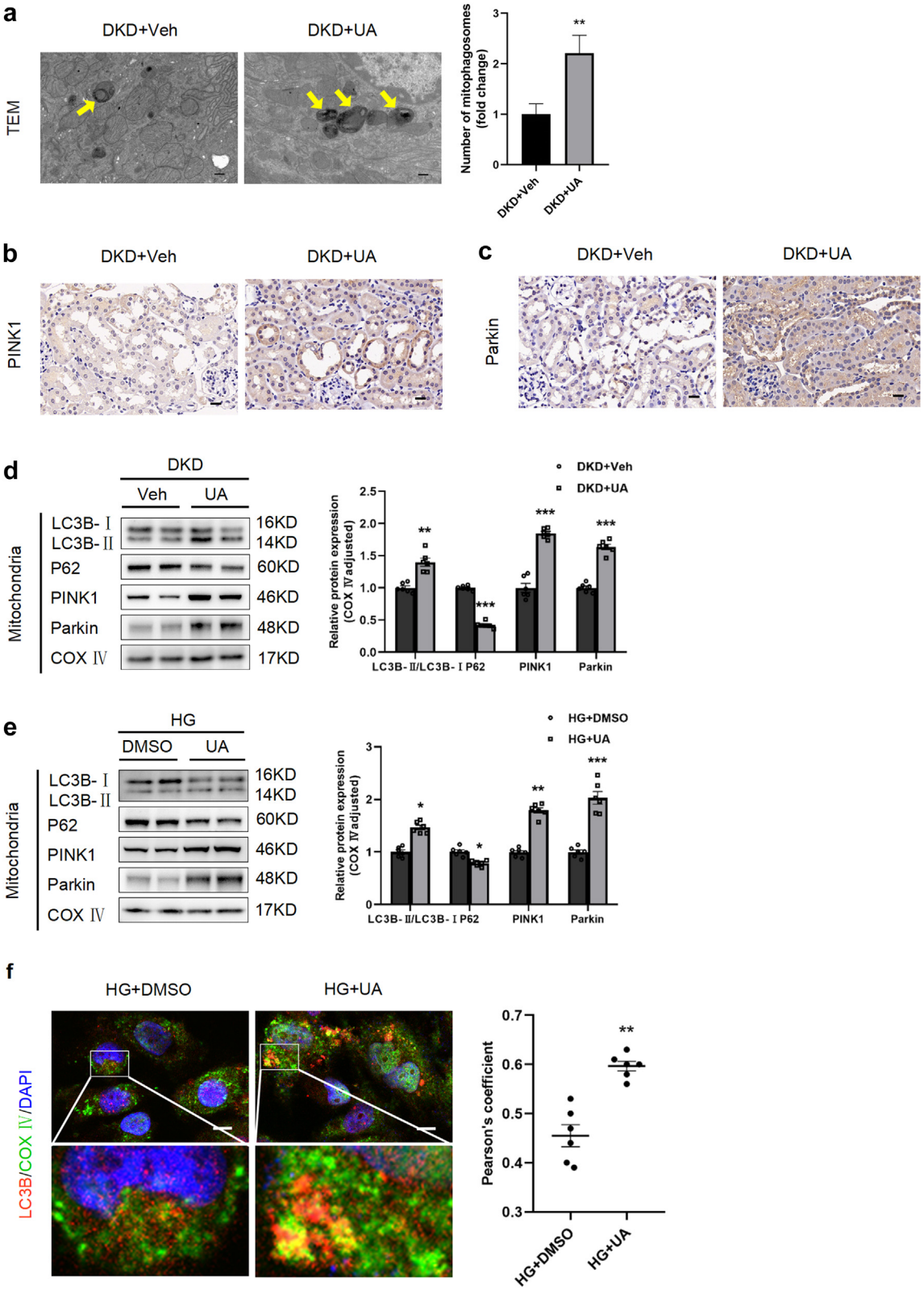

Figure 3. Mitophagy activation attenuated renal tubular injury and tubulointerstitial inflammation in DKD. (a) Representative transmission electron microscopy (TEM) images of intracellular mitophagosomes (arrows) in renal tubular epithelial cells from the 2 groups of mice. Scale bars, 400 nm. (b) Representative images of PINK1 immunohistochemical staining. Scale bars, 20 μm. (c) Representative images of Parkin immunohistochemical staining. Scale bars, 20 μm. (d) Representative western blotting images and densitometric analysis of LC3B, P62, PINK1, and Parkin in kidney. (e) Representative western blotting images and densitometric analysis of LC3B, P62, PINK1, and Parkin in HK-2 cells. (f) Representative confocal microscopic images and the Pearson correlation coefficient showing the colocalization of LC3B and COX IV in HK-2 cells. Nuclei were revealed using DAPI staining. Scale bars, 10 μm. (Continued)

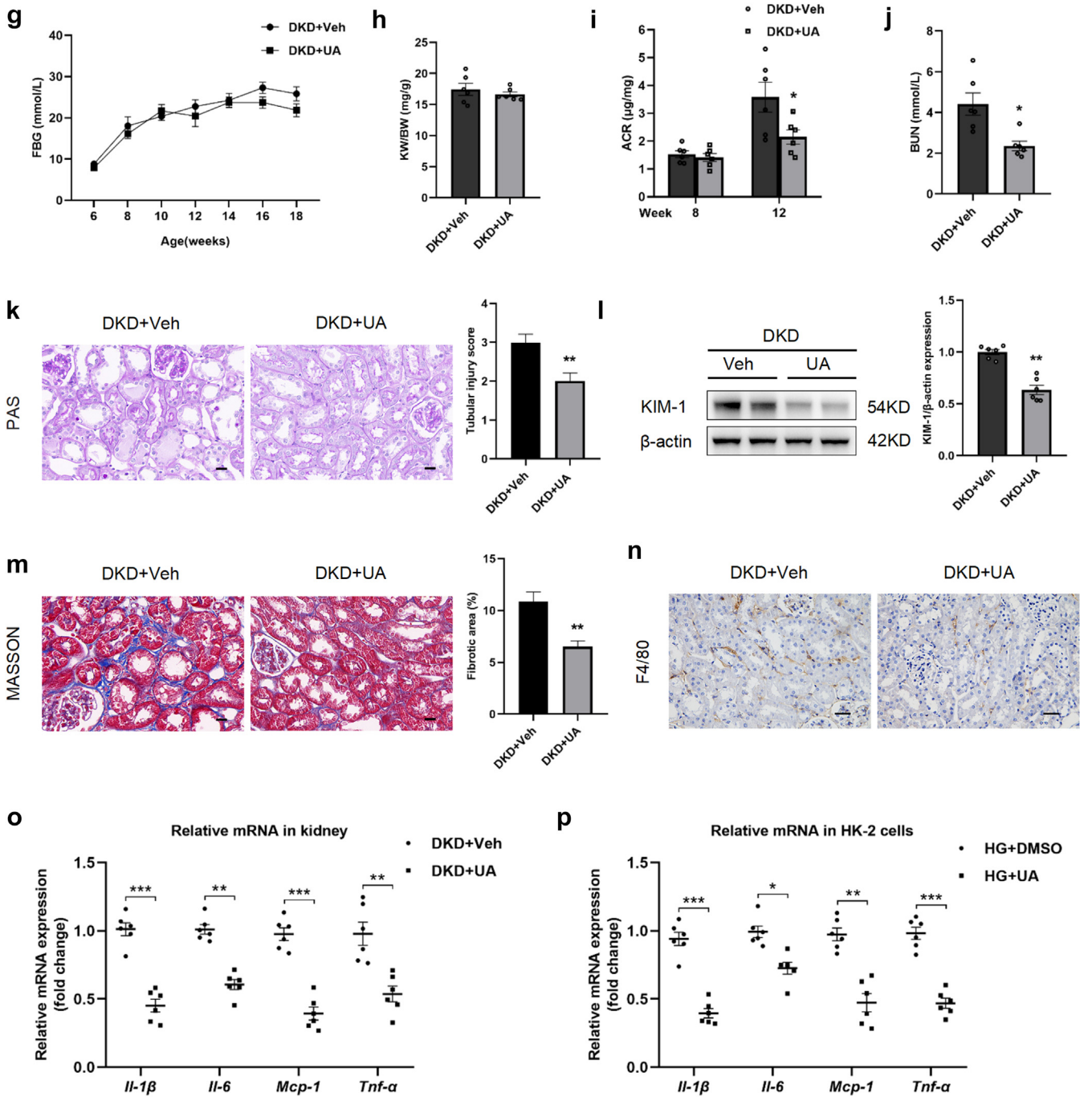

Figure 3. (Continued) (g) The levels of fasting blood glucose (FBG). (h) Kidney weight-to-body weight ratio (KW/BW). (i) Urinary ACR. (j) The blood urea nitrogen (BUN) levels. (k) Representative images of Periodic acid-Schiff (PAS) staining of kidney sections. Scale bars, 20 μm. (l) Representative western blotting images and densitometric analysis of KIM-1 in kidney. (m) Representative images of Masson's trichrome staining and the quantitative analysis of fibrotic area. Scale bar, 20 μm. (n) Representative images of F4/80 immunohistochemical staining. Scale bars, 20 μm. (o) Real-time polymerase chain reaction analysis of the mRNA expression levels of *Il-1β*, *Il-6*, *Mcp-1*, and *Tnf-α* in kidney. (p) Real-time polymerase chain reaction analysis of the mRNA expression levels of *Il-1β*, *Il-6*, *Mcp-1*, and *Tnf-α* in HK-2 cells. All data above are represented as means ± SEM. $n = 6$, $^{*}P < 0.05$, $^{**}P < 0.01$, $^{***}P < 0.001$. ACR, albumin-to-creatinine ratio; DAPI, 4′,6-diamidino-2-phenylindole; DKD, diabetic kidney disease; DMSO, dimethyl sulfoxide; HG, high glucose; MCP-1, monocyte chemoattractant protein-1; PAS, Periodic acid-Schiff staining; TNF-α, tumor necrosis factor-α; UA, urolithin A; Veh, vehicle.

indicated that PINK1 and Parkin expressions were markedly increased (Figure 4e and f). LC3B-II/LC3B-I, PINK1, and Parkin expressions were increased, whereas P62 expression was decreased with *Trpc6* knockdown lentivirus treatment in DKD mice (Figure 4g). The same trend was observed in HG-stimulated HK-2 cells with *Trpc6* siRNA treatment (Figure 4h). Compared with the HG + si-*Trpc6* + si-*NC* group, protein levels of LC3B-II/LC3B-I, PINK1, and Parkin were markedly reduced in the HG + si-*Trpc6* +

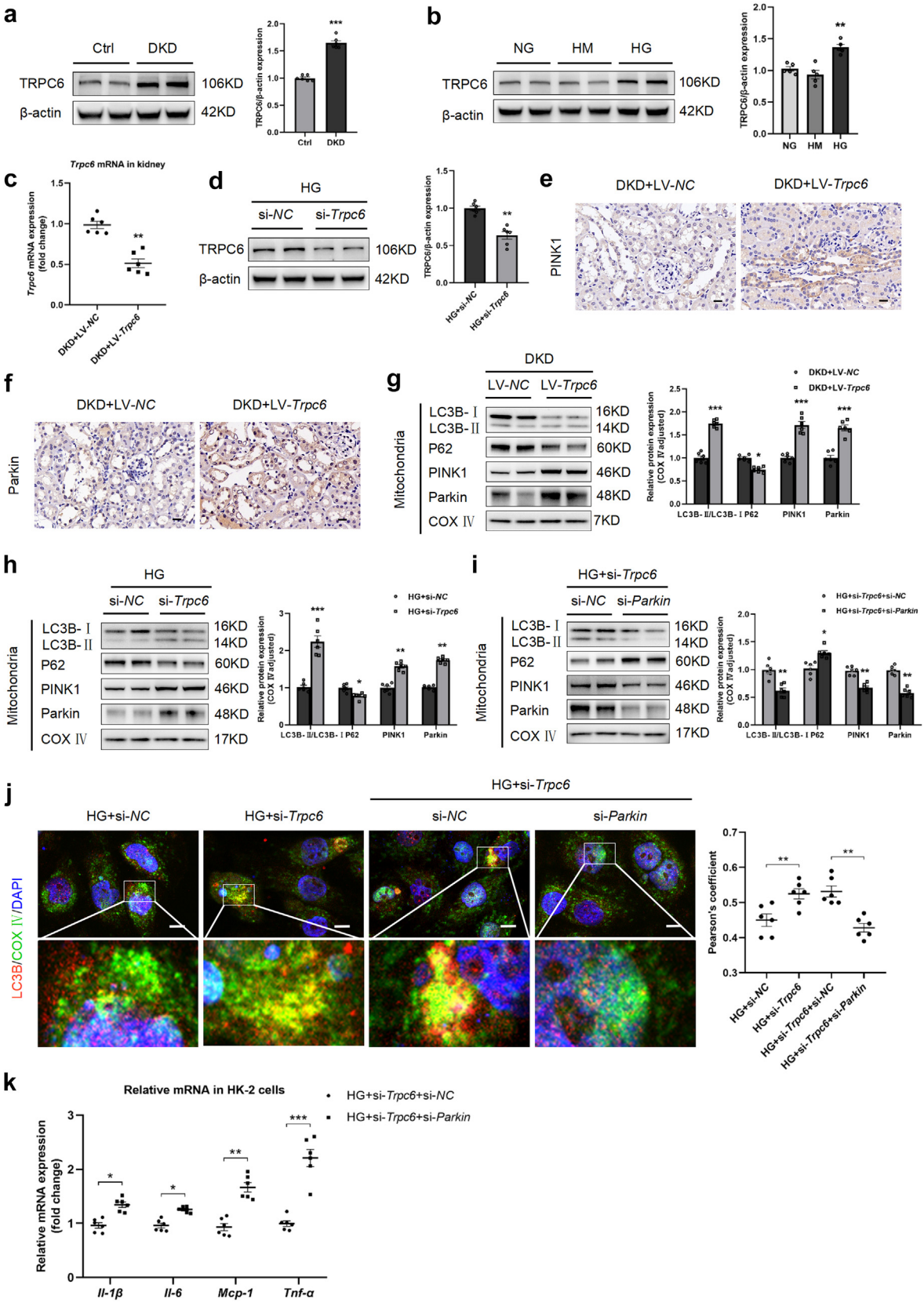

Figure 4. TRPC6 inhibited mitophagy in DKD. (a) Representative western blotting images and densitometric analysis of TRPC6 in kidney. (b) Representative western blotting images and densitometric analysis TRPC6 and in HK-2 cells. (c) Real-time polymerase chain reaction analysis of the mRNA expression level of *Trpc6* in kidney. (d) Representative western blotting images and densitometric analysis of TRPC6 in HK-2 cells. (e) Representative images of PINK1 immunohistochemical staining. Scale bars, 20 μm. (f) Representative images of Parkin immunohistochemical staining. Scale bars, 20 μm. (g) Representative western blotting images and densitometric analysis of LC3B, P62, PINK1, and Parkin in kidney. (h) Representative western blotting images and densitometric analysis of LC3B, P62, PINK1, and Parkin in HK-2 cells. (Continued)

si-*Parkin* group, whereas P62 expression was increased (Figure 4i). Immunofluorescence results revealed increased LC3B and COX IV fusion in HG-stimulated HK-2 cells with *Trpc6* siRNA administration, and the increase was almost abrogated by *Parkin* siRNA (Figure 4j). Concomitantly, there were significant increases in mRNA expression levels of renal inflammatory cytokines in the HG + si-*Trpc6* + si-*Parkin* group (Figure 4k). These findings demonstrated that TRPC6 inhibited tubular mitophagy in DKD.

Trpc6 Knockdown Attenuated Renal Tubular Injury and Tubulointerstitial Inflammation

Then, the potential effect of TRPC6 on tubular injury and tubulointerstitial inflammation was explored. We found that there were no differences in FBG levels and kidney weight-to-body weight ratio in DKD mice with LV-*Trpc6* or LV-*NC* administration (Figure 5a and b). However, urinary albumin-to-creatinine ratio and blood urea nitrogen decreased after LV-*Trpc6* injection (Figure 5c and d). More importantly, the tubular injury was significantly ameliorated, revealed by Periodic acid-Schiff staining and the kidney tubular injury marker, KIM-1 (Figure 5e and f). Meanwhile, Masson's trichrome staining revealed ameliorated tubulointerstitial fibrosis (Figure 5g). More mitophagosomes were observed in DKD mice with LV-*Trpc6* administration by transmission electron microscopy (Figure 5h). F4/80-positive cells and inflammatory cytokines were decreased in DKD + LV-*Trpc6* mice (Figure 5i and j). In addition, the same pattern was found in HG-stimulated HK-2 cells with *Trpc6* siRNA treatment (Figure 5k). These findings demonstrate that *Trpc6* knockdown attenuated renal tubular injury and tubulointerstitial inflammation.

Calpain-1 Activation was Associated With TRPC6-Mediated Intracellular Ca^{2+} Influx

Next, the exact mechanism of TRPC6-mediated mitophagy regulation was investigated. Previous studies indicated that calpain-1 is a specific Ca^{2+}-sensitive intracellular protease that may be associated with autophagy. We thus hypothesized that calpain-1 activation was involved in the TRPC6-mediated mitophagy inhibition. As expected, we found that calpain-1 expression was significantly increased in DKD mice and HG-stimulated HK-2 cells (Figure 6a and b). Meanwhile, decreased expression of calpain-1 protein was observed when *Trpc6* was knocked down (Figure 6c and d). Interestingly, we found that calpain-1 expression decreased with BAPTA (a specific Ca^{2+} chelator) treatment (Figure 6e). Immunofluorescence results revealed that the expression of calpain-1 was consistent with the level of Ca^{2+} (Figure 6f). These findings suggest that calpain-1 is upregulated in DKD and is associated with increased Ca^{2+} influx, which is mediated by TRPC6.

Calpain-1 Inhibition Activated Mitophagy

To investigate the functional effect of calpain-1 on mitophagy, we used calpeptin (a calpain-1 inhibitor) to inhibit calpain-1 (Figure 7a and b). Interestingly, the expressions of LC3B-II/LC3B-I, PINK1, and Parkin were increased whereas P62 expression was reduced in the HG + calpeptin group (Figure 7c). Compared with the HG + calpeptin + si-*NC* group, protein levels of LC3B-II/LC3B-I, PINK1, and Parkin were markedly reduced in the HG + calpeptin + si-*Parkin* group, whereas P62 expression was increased (Figure 7d). Colocalization of LC3B with COX IV was increased with calpeptin treatment, and the increase was almost abrogated by *Parkin* siRNA (Figure 7e). Concomitantly, there were significant increases in mRNA expression levels of renal inflammatory cytokines in the HG + calpeptin + si-*Parkin* group (Figure 7f). These results demonstrate that calpain-1 inhibition activated mitophagy.

DISCUSSION

Here, the exact molecular mechanism underlying mitophagy abnormality-mediated tubulointerstitial inflammation in DKD was systemically studied. We elucidated the crucial role of TRPC6 in mitophagy inhibition-induced renal tubulointerstitial inflammation in DKD. Mechanistically, TRPC6-impaired mitophagy through the activation of calpain-1 and promoted renal tubulointerstitial inflammation under DKD condition (Figure 8). Our findings not only represent novel insights into the pathogenesis of DKD, but also provide a promising therapeutic strategy for delaying the progression of DKD.

Although some progress has been made, the exact mechanism of the pathogenesis and progression in DKD has not been fully understood. DKD has

Figure 4. (Continued) (i) Representative western blotting images and densitometric analysis of LC3B, P62, PINK1, and Parkin in HK-2 cells. (j) Representative confocal microscopic images and the Pearson correlation coefficient showing the colocalization of LC3B and COX IV in HK-2 cells. Nuclei were revealed using DAPI staining. Scale bars, 10 μm. (k) Real-time polymerase chain reaction analysis of the mRNA expression levels of *Il-1β*, *Il-6*, *Mcp-1*, and *Tnf-α* in HK-2 cells. All data above are represented as means ± SEM. $n = 6$, $^{*}P < 0.05$, $^{**}P < 0.01$, $^{***}P < 0.001$. DAPI, 4′,6-diamidino-2-phenylindole; DKD, diabetic kidney disease; HG, high glucose; IL, interleukin; LV, lentivirus; MCP-1, monocyte chemoattractant protein-1; NC, negative control; TNF-α, tumor necrosis factor-α; TRPC6, transient receptor potential cation channel subfamily C member 6.

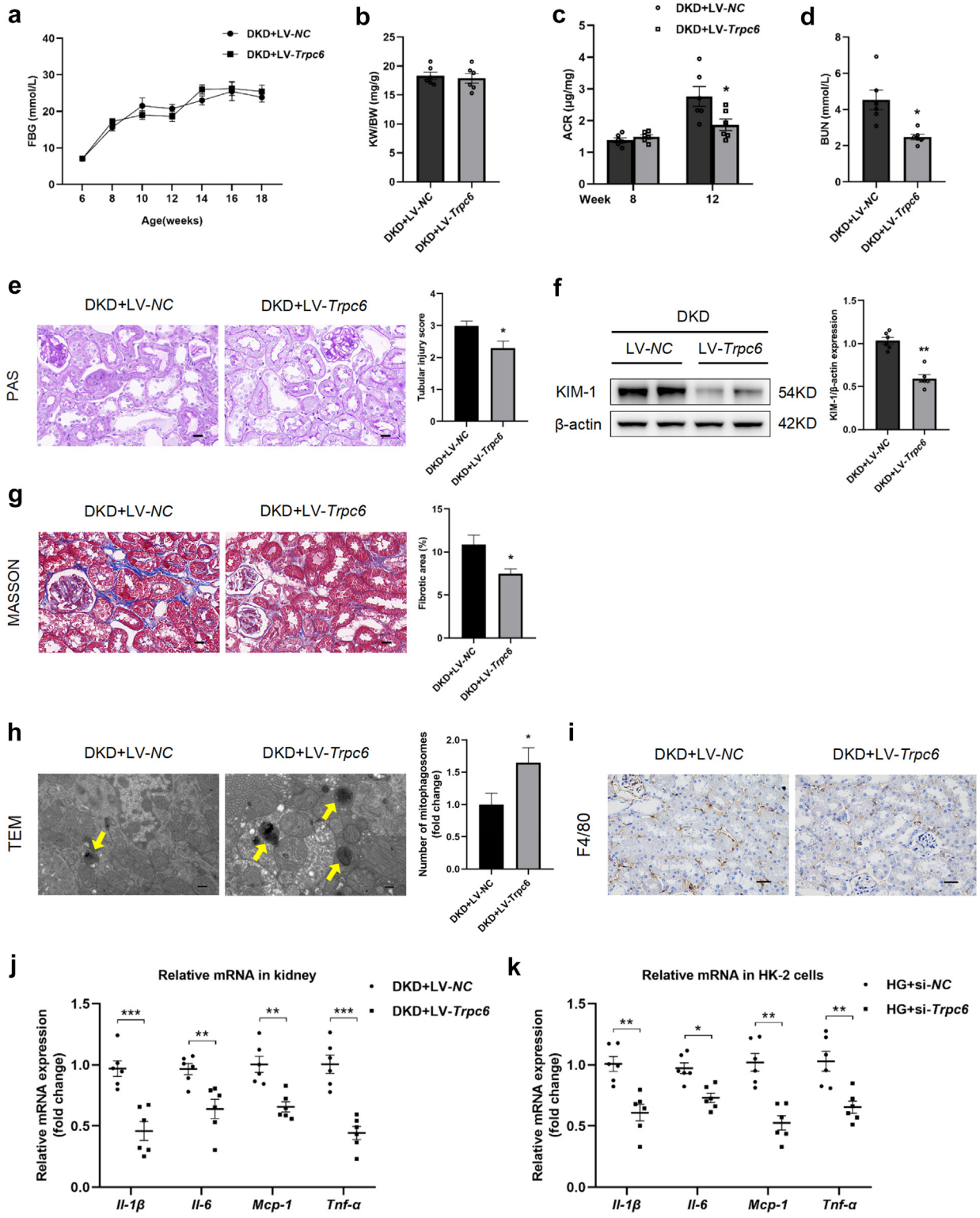

Figure 5. *Trpc6* knockdown attenuated renal tubular injury and tubulointerstitial inflammation. (a) The levels of fasting blood glucose (FBG). (b) Kidney weight-to-body weight ratio (KW/BW). (c) Urinary ACR. (d) The blood urea nitrogen (BUN) levels. (e) Representative images of Periodic acid-Schiff (PAS) staining of kidney sections. Scale bars, 20 μm. (f) Representative western blotting images and densitometric analysis of KIM-1 in kidney. (g) Representative images of Masson's trichrome staining and the quantitative analysis of fibrotic area. Scale bar, 20 μm. (h) Representative transmission electron microscopy (TEM) images of intracellular mitophagosomes (arrows) in renal tubular epithelial cells from the 2 groups of mice. Scale bars, 400 nm. (i) Representative images of F4/80 immunohistochemical staining. Scale bars, 20 μm. (j) Real-time polymerase chain reaction analysis of the mRNA expression levels of *Il-1β*, *Il-6*, *Mcp-1*, and *Tnf-α* in kidney. (k) Real-time polymerase chain reaction analysis of the mRNA expression levels of *Il-1β*, *Il-6*, *Mcp-1* and *Tnf-α* in HK-2 cells. All data above are represented as means ± SEM. $n = 6$, $^{*}P < 0.05$, $^{**}P < 0.01$, $^{***}P < 0.001$. ACR, albumin-to-creatinine ratio. IL, interleukin; MCP-1, monocyte chemoattractant protein-1; TNF-α, tumor necrosis factor-α; Trpc6, transient receptor potential cation channel subfamily C member 6.

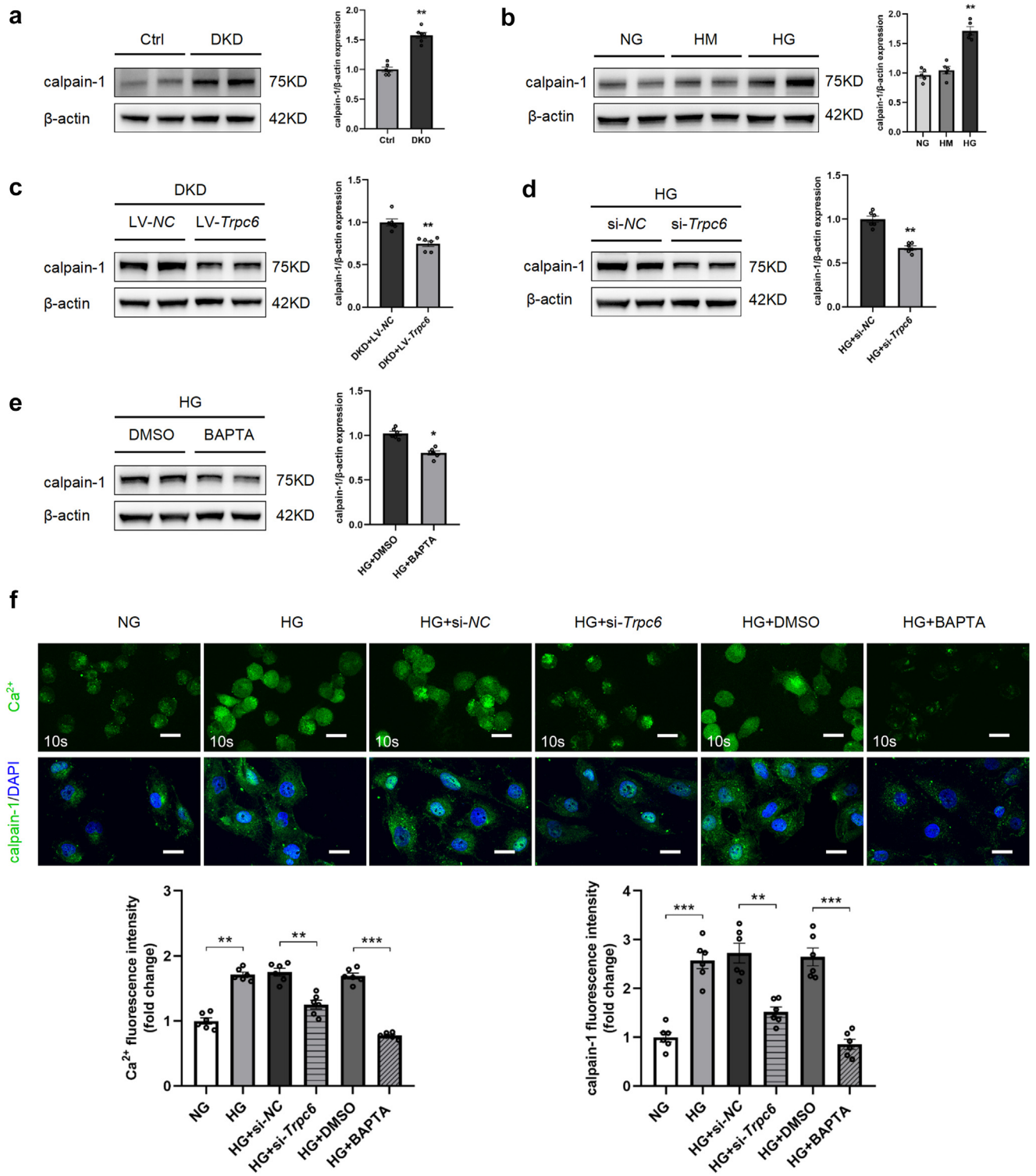

Figure 6. Calpain-1 activation was associated with TRPC6-mediated intracellular Ca^{2+} influx. (a) Representative western blotting images and densitometric analysis of calpain-1 in kidney. (b) Representative western blotting images and densitometric analysis of calpain-1 in HK-2 cells. (c) Representative western blotting images and densitometric analysis of calpain-1 in kidney. (d) Representative western blotting images and densitometric analysis of calpain-1 in HK-2 cells. (e) Representative western blotting images and densitometric analysis of calpain-1 in HK-2 cells. (f) Representative confocal microscopic images and quantitative analysis showing the expressions of Ca^{2+} and calpain-1 in HK-2 cells. Nuclei were revealed using DAPI staining. Scale bars, 20 μm. All data above are represented as means ± SEM. $n = 6$, $^{*}P < 0.05$, $^{**}P < 0.01$, $^{***}P < 0.001$. DAPI, 4′,6-diamidino-2-phenylindole; TRPC6, transient receptor potential cation channel subfamily C member 6.

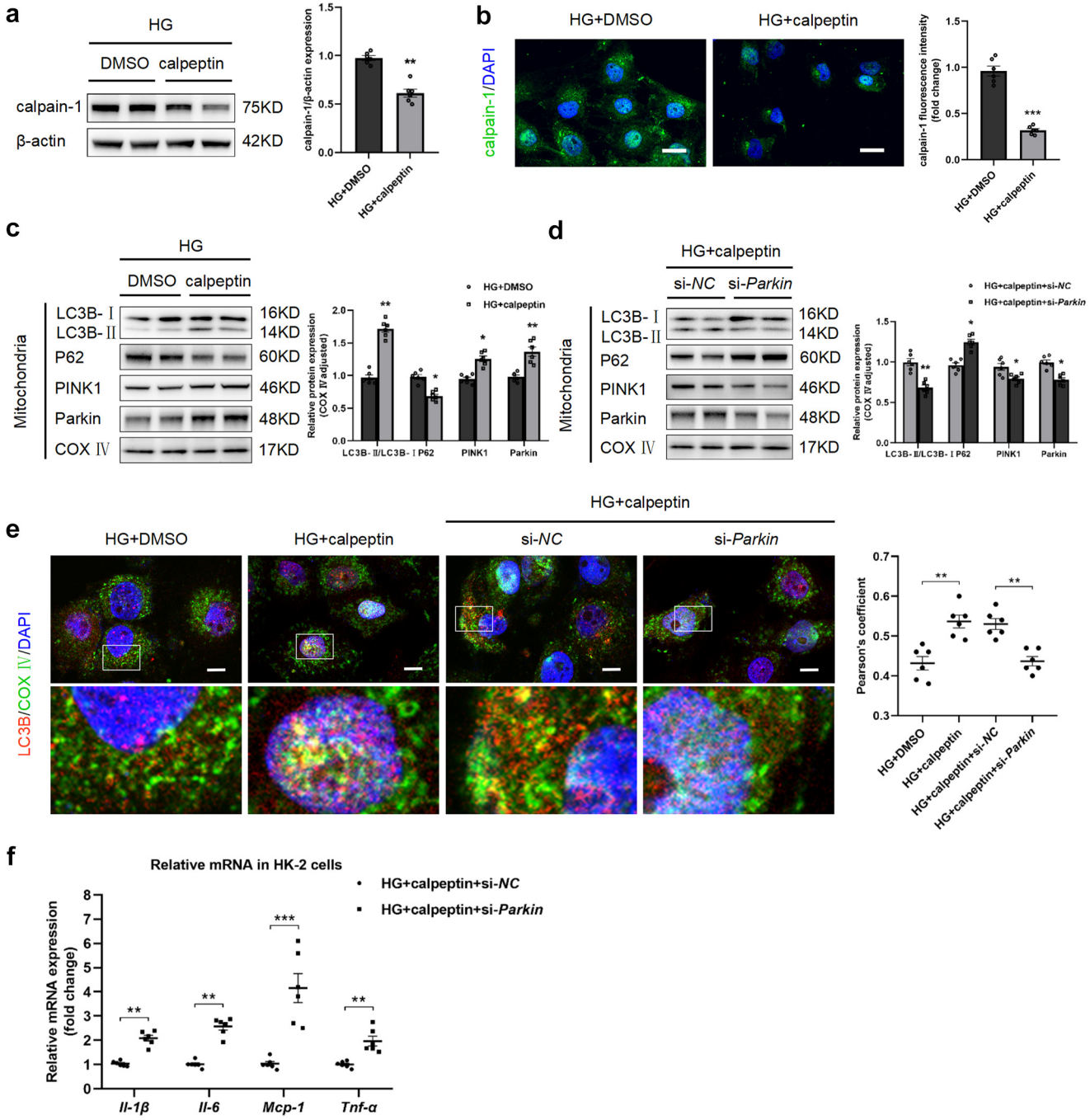

Figure 7. Calpain-1 inhibition activated mitophagy. (a) Representative western blotting images and densitometric analysis of calpain-1 in HK-2 cells. (b) Representative confocal microscopic images and quantitative analysis showing the expression of calpain-1 in HK-2 cells. Nuclei were revealed using DAPI staining. Scale bars, 20 μm. (c) Representative western blotting images and densitometric analysis of LC3B, P62, PINK1, and Parkin in HK-2 cells. (d) Representative western blotting images and densitometric analysis of LC3B, P62, PINK1, and Parkin in HK-2 cells. (e) Representative confocal microscopic images and the Pearson correlation coefficient showing the colocalization of LC3B and COX IV in HK-2 cells. Nuclei were revealed using DAPI staining. Scale bars, 10 μm. (f) Real-time polymerase chain reaction analysis of the mRNA expression levels of *Il-1β*, *Il-6*, *Mcp-1*, and *Tnf-α* in HK-2 cells. All data above are represented as means ± SEM. $n = 6$, $^{*}P < 0.05$, $^{**}P < 0.01$, $^{***}P < 0.001$. DAPI, 4′,6-diamidino-2-phenylindole; IL, interleukin; MCP-1, monocyte chemoattractant protein-1; TNF-α, tumor necrosis factor-α.

previously been regarded as a glomerular disease, and the damage of renal tubules has been considered secondary to the glomerular injury. However, a growing body of evidence has demonstrated that tubulointerstitial damage in DKD starts from a primary tubular injury.[22] Tubulointerstitial inflammation, one of the important pathological features of DKD, is a critical mediator in the pathophysiology of DKD progression, eventually leading to end-stage renal disease.[23] Our data revealed the increases in inflammatory cytokines

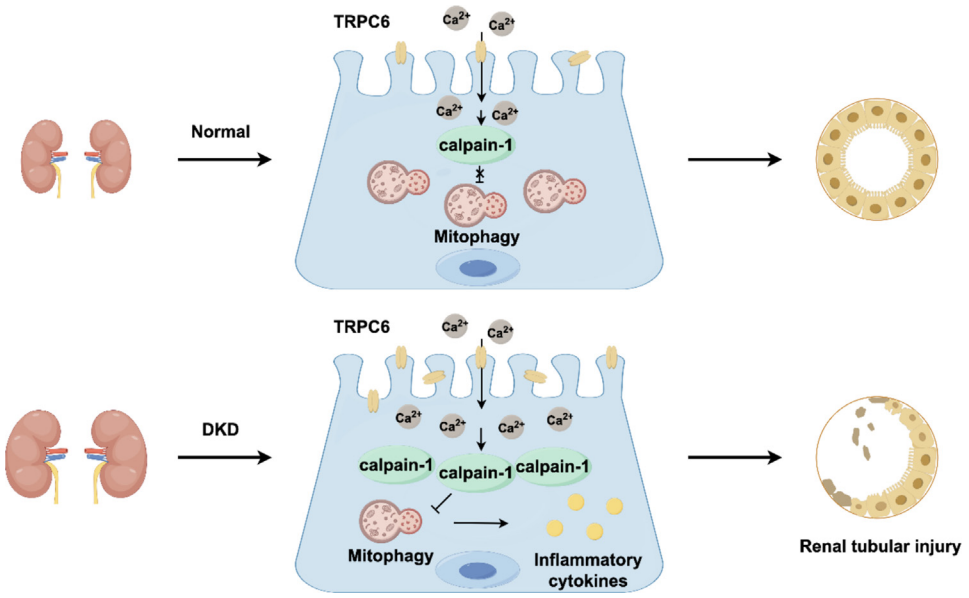

Figure 8. Schematic illustration of the mechanism of upregulated TRPC6 affecting renal tubulointerstitial inflammation in DKD. In tubular epithelial cells under the condition of DKD, the increased inflammatory cytokines release is associated with increased TRPC6 expression. Increased TRPC6 activates calpain-1 by Ca^{2+} influx, leading to the inhibition of mitophagy. Damaged or dysfunctional mitochondria cannot be removed. Then, the release of increased inflammatory cytokines results in renal tubular injury. DKD, diabetic kidney disease; TRPC6, transient receptor potential cation channel subfamily C member 6.

under DKD conditions, and the histopathological observation indicated renal tubular lesions and tubulointerstitial fibrosis. However, the precise regulatory pathway for these effects remains unclear.

Mitophagy means that cells selectively wrap and degrade damaged mitochondria through an autophagy mechanism, thus maintaining mitochondrial homeostasis.[24,25] It is well-known that mitophagy is primarily achieved through the ubiquitin-dependent (PINK1/Parkin) pathway: PINK1 selectively recruits the ubiquitin ligase Parkin to damaged mitochondria. Activated Parkin catalyzes the formation of polyubiquitin chains that recruit adaptor proteins. These adaptor proteins induce the formation of autophagosome by binding to LC3 proteins on autophagosome membranes.[26-28] Previous studies identified several important adaptor proteins as mitophagy receptors, including P62.[29] Here, as a specific cargo receptor for autophagy, P62 was found to be significantly elevated under the condition of DKD, indicating the inhibition of mitophagic flux. In fact, growing evidence demonstrated that the transcription of P62 is also markedly increased during conditions in which selective autophagy substrates accumulate. Given the complex effects of P62, the function of enhanced P62 accumulation in DKD needs further investigation.

Damaged mitochondria fail to supply sufficient ATP, causing an energetic deficit, resulting in atrophy or dedifferentiation of kidney tubule cells.[30] Severe mitochondrial damage and dysfunction of mitochondrial clearance also leads to a leakage of the mitochondrial DNA into the tubular cytosol, activation of the cytosolic cGAS-stimulator of interferon genes DNA sensing pathway, and contributes to cytokine expression and immune cell recruitment.[31] Furthermore, defective mitochondria fail to maintain the proton gradient across the inner mitochondrial membrane and are the main source of reactive oxygen species, aggravating inflammation and tubulointerstitial fibrosis.[32] Restoring PINK1/Parkin-mediated mitophagy indeed ameliorates tubulointerstitial injury in DKD.[33] In this study, we found impairment of PINK1/Parkin-mediated mitophagy under the condition of DKD, which is consistent with previous studies.[34] Our data demonstrated that mitophagy activation attenuates the significant tubulointerstitial inflammation, thereby alleviating tubular injury in DKD. Collectively, these findings encourage us to explore the exact mechanism of mitophagy abnormality in mediating DKD-induced tubulointerstitial inflammation.

TRPC6 was demonstrated to be associated with pathological changes in DKD, such as podocyte injury.[35] Indeed, TRPC6 participates in a variety of pathological processes, such as cell proliferation, apoptosis, fibrosis, and inflammation.[14,16,36,37] Here, we innovatively found that knockdown of TRPC6 effectively alleviated tubulointerstitial inflammation in DKD mice through mitophagy regulation. Hou *et al.*[38] identified that TRPC6-mediated Ca^{2+} influx plays a

novel role in suppressing cytoprotective autophagy triggered by oxidative stress in primary TECs. In this study, we found that mitophagy could be inhibited by the activated TRPC6 in DKD. Therefore, TRPC6-mediated mitophagy plays a vital role in the development tubulointerstitial inflammation under the condition of DKD.

What is the exact mechanism of TRPC6-mediated mitophagy in DKD? Given that TRPC6 is a Ca^{2+}-permeable nonselective cation channel and calpain is Ca^{2+}-sensitive intracellular protease, it is not difficult to understand that mitophagy may be regulated by TRPC6-calpain-1 axis. Calpains are a family of Ca^{2+}-dependent cysteine proteases. Previously, calpains were proven to be involved in a variety of physiological and pathological processes, including but not limited to, cell proliferation, cytoskeletal degradation, apoptosis, autophagy, and inflammation.[39-43] Calpain-1, one of the members of the calpain superfamily, has been found to be involved in impaired podocyte autophagy.[17] In our study, we observed inhibited calpain-1 expression in the *in vivo* and *in vitro* models of DKD with TRPC6 deletion, and blockade of Ca^{2+} by BAPTA diminished the expression of calpain-1. More importantly, when the TRPC6-calpain-1 axis is intervened, tubular mitophagy undergoes corresponding characteristic changes. Hence, our experiments identify a novel regulatory mechanism that links TRPC6-calpain-1 axis and mitophagy.

Under some pathological condition, the participation of calpain in the dysfunction of mitophagy has been found, such as retinal ischemic injury, heart ischemia-reperfusion injury and neuronal oxidative injury.[44,45] The mechanism by which calpain impairs mitophagy is complicated and involves several components of mitophagy process. For instance, Chen *et al*.[45] demonstrated that activation of calpain degrades cytosolic beclin-1 and decreases the content of LC3B, leading to mitophagy defects. Moreover, calpain was found to downregulate OPA1-mediated mitophagy.[46] Despite the crucial role of calpain-1 in mitophagy abnormality, further research is needed to ascertain molecular mechanisms responsible for the effect of calpain-1 on mitophagy in DKD.

In summary, we have discovered an important role for TRPC6-calpain-1 axis in inciting renal tubulointerstitial inflammation in the kidney via disrupting mitophagy, highlighting the versatile regulatory mechanisms of TRPC6 in modulating inflammation in DKD. These findings provide unique insights into interdigitating mechanisms of tubular injury and tubulointerstitial inflammation in DKD. Interrupting this broad, vertically integrated TRPC6-mitophagy signaling cascade represents a promising therapeutic target for DKD.

DISCLOSURE

All the authors declared no competing interests.

ACKNOWLEDGMENTS

This work was supported by the National Natural Science Foundation of China (82000648), the Outstanding Youth Cultivation Foundation of Southeast University (2021ZDYYYQPY07), the Fundamental Research Funds for the Central Universities (2242023K40046), the Innovative and Entrepreneurial Talent (Doctor) of Jiangsu Province; the Natural Science Foundation of Shandong Province (ZR2022MH161), Taishan Scholar Program of Shandong Province (NO.tstp20230665), the Qingdao Medical and Health Research Program Project (2021-WJZD189), the Qingdao Key Health Discipline Development Fund, and the Qingdao Key Clinical Specialty Elite Discipline.

SUPPLEMENTARY MATERIAL

Supplementary File (PDF)

Figure S1. The expression of TRPC6 was markedly decreased in the mice with *Trpc6* knockdown lentivirus administration.

REFERENCES

1. Tuttle KR, Agarwal R, Alpers CE, et al. Molecular mechanisms and therapeutic targets for diabetic kidney disease. *Kidney Int*. 2022;102:248–260. https://doi.org/10.1016/j.kint.2022.05.012
2. Tang SCW, Yiu WH. Innate immunity in diabetic kidney disease. *Nat Rev Nephrol*. 2020;16:206–222. https://doi.org/10.1038/s41581-019-0234-4
3. Jiang WJ, Xu CT, Du CL, et al. Tubular epithelial cell-to-macrophage communication forms a negative feedback loop via extracellular vesicle transfer to promote renal inflammation and apoptosis in diabetic nephropathy. *Theranostics*. 2022;12:324–339. https://doi.org/10.7150/thno.63735
4. Yao L, Liang X, Qiao Y, Chen B, Wang P, Liu Z. Mitochondrial dysfunction in diabetic tubulopathy. *Metabolism*. 2022;131:155195. https://doi.org/10.1016/j.metabol.2022.155195
5. Wang S, Long H, Hou L, et al. The mitophagy pathway and its implications in human diseases. *Signal Transduct Target Ther*. 2023;8:304. https://doi.org/10.1038/s41392-023-01503-7
6. Wang Y, Song D, Tang L. Mitophagy, inflammasomes and their interaction in kidney diseases: a comprehensive review of experimental studies. *J Inflamm Res*. 2023;16:1457–1469. https://doi.org/10.2147/jir.S402290
7. Yao L, Liang X, Liu Y, et al. Non-steroidal mineralocorticoid receptor antagonist finerenone ameliorates mitochondrial dysfunction via PI3K/Akt/eNOS signaling pathway in diabetic tubulopathy. *Redox Biol*. 2023;68:102946. https://doi.org/10.1016/j.redox.2023.102946

8. Ahmad AA, Draves SO, Rosca M. Mitochondria in diabetic kidney disease. *Cells*. 2021;10:2945. https://doi.org/10.3390/cells10112945
9. Xiao L, Xu X, Zhang F, et al. The mitochondria-targeted antioxidant MitoQ ameliorated tubular injury mediated by mitophagy in diabetic kidney disease via Nrf2/PINK1. *Redox Biol*. 2017;11:297–311. https://doi.org/10.1016/j.redox.2016.12.022
10. Saxena S, Mathur A, Kakkar P. Critical role of mitochondrial dysfunction and impaired mitophagy in diabetic nephropathy. *J Cell Physiol*. 2019;234:19223–19236. https://doi.org/10.1002/jcp.28712
11. Li C, Li L, Yang M, et al. PACS-2 ameliorates tubular injury by facilitating endoplasmic reticulum-mitochondria contact and mitophagy in diabetic nephropathy. *Diabetes*. 2022;71:1034–1050. https://doi.org/10.2337/db21-0983
12. Colya N, Englisch FP, Tschernig T. TRPC channels in the physiology and pathophysiology of the renal tubular system: what do we know? *Int J Mol Sci*. 2022;24:181. https://doi.org/10.3390/ijms
13. Staruschenko A. TRPC6 in diabetic kidney disease: good guy or bad guy? *Kidney Int*. 2019;95:256–258. https://doi.org/10.1016/j.kint.2018.10.027
14. Fu Y, Wang C, Zhang D, et al. Increased TRPC6 expression is associated with tubular epithelial cell proliferation and inflammation in diabetic nephropathy. *Mol Immunol*. 2018;94:75–81. https://doi.org/10.1016/j.molimm.2017.12.014
15. Zhang S, Wang H, Liu Y, et al. Tacrolimus ameliorates tubulointerstitial inflammation in diabetic nephropathy via inhibiting the NFATc1/TRPC6 pathway. *J Cell Mol Med*. 2020;24:9810–9824. https://doi.org/10.1111/jcmm.15562
16. Ma R, Wang Y, Xu Y, et al. Tacrolimus protects podocytes from apoptosis via downregulation of TRPC6 in diabetic nephropathy. *J Diabetes Res*. 2021;2021:1–11. https://doi.org/10.1155/2021/8832114
17. Salemkour YYD, Dionet L, Hart DC, et al. Podocyte injury in diabetic kidney disease in a mouse model involves TRPC6-mediated calpain activation impairing autophagy. *J Am Soc Nephrol*. 2023;34:1823–1842. https://doi.org/10.1681/ASN.0000000000000212
18. Hou X, Xiao H, Zhang Y, et al. Transient receptor potential channel 6 knockdown prevents apoptosis of renal tubular epithelial cells upon oxidative stress via autophagy activation. *Cell Death Dis*. 2018;9:1015. https://doi.org/10.1038/s41419-018-1052-5
19. Sakai S, Yamamoto T, Takabatake Y, et al. Proximal tubule autophagy differs in type 1 and 2 diabetes. *J Am Soc Nephrol*. 2019;30:929–945. https://doi.org/10.1681/asn.2018100983
20. Wu S, Lu Q, Ding Y, et al. Hyperglycemia-driven inhibition of AMP-activated protein kinase α2 induces diabetic cardiomyopathy by promoting mitochondria-associated endoplasmic reticulum membranes in vivo. *Circulation*. 2019;139:1913–1936. https://doi.org/10.1161/circulationaha.118.033552
21. Dong Y, Zhang Q, Wen J, et al. Ischemic duration and frequency determines AKI-to-CKD progression monitored by dynamic changes of tubular biomarkers in IRI mice. *Front Physiol*. 2019;10:153. https://doi.org/10.3389/fphys.2019.00153
22. Chang J, Yan J, Li X, Liu N, Zheng R, Zhong Y. Update on the mechanisms of tubular cell injury in diabetic kidney disease. *Front Med (Lausanne)*. 2021;8:661076. https://doi.org/10.3389/fmed.2021.661076
23. Rayego-Mateos S, Rodrigues-Diez RR, Fernandez-Fernandez B, et al. Targeting inflammation to treat diabetic kidney disease: the road to 2030. *Kidney Int*. 2023;103:282–296. https://doi.org/10.1016/j.kint.2022.10.030
24. Choi ME. Autophagy in kidney disease. *Annu Rev Physiol*. 2020;82:297–322. https://doi.org/10.1146/annurev-physiol-021119-034658
25. Lu Y, Li Z, Zhang S, Zhang T, Liu Y, Zhang L. Cellular mitophagy: mechanism, roles in diseases and small molecule pharmacological regulation. *Theranostics*. 2023;13:736–766. https://doi.org/10.7150/thno.79876
26. Tang C, Livingston MJ, Liu Z, Dong Z. Autophagy in kidney homeostasis and disease. *Nat Rev Nephrol*. 2020;16:489–508. https://doi.org/10.1038/s41581-020-0309-2
27. Wang L, Lu G, Shen H-M. The long and the short of PTEN in the regulation of mitophagy. *Front Cell Dev Biol*. 2020;8:299. https://doi.org/10.3389/fcell.2020.00299
28. Dai W, Lu H, Chen Y, Yang D, Sun L, He L. The loss of mitochondrial quality control in diabetic kidney disease. *Front Cell Dev Biol*. 2021;9:706832. https://doi.org/10.3389/fcell.2021.706832
29. Wang Y, Tang C, Cai J, et al. PINK1/Parkin-mediated mitophagy is activated in cisplatin nephrotoxicity to protect against kidney injury. *Cell Death Dis*. 2018;9:1113. https://doi.org/10.1038/s41419-018-1152-2
30. Doke T, Susztak K. The multifaceted role of kidney tubule mitochondrial dysfunction in kidney disease development. *Trends Cell Biol*. 2022;32:841–853. https://doi.org/10.1016/j.tcb.2022.03.012
31. Chung KW, Dhillon P, Huang S, et al. Mitochondrial damage and activation of the STING pathway lead to renal inflammation and fibrosis. *Cell Metab*. 2019;30:784–799.e5. https://doi.org/10.1016/j.cmet.2019.08.003
32. Han Y, Xu X, Tang C, et al. Reactive oxygen species promote tubular injury in diabetic nephropathy: the role of the mitochondrial ros-txnip-nlrp3 biological axis. *Redox Biol*. 2018;16:32–46. https://doi.org/10.1016/j.redox.2018.02.013
33. Sun J, Zhu H, Wang X, Gao Q, Li Z, Huang H. CoQ10 ameliorates mitochondrial dysfunction in diabetic nephropathy through mitophagy. *J Endocrinol*. 2019;240:445–465. https://doi.org/10.1530/joe-18-0578
34. Liu L, Bai F, Song H, et al. Upregulation of TIPE1 in tubular epithelial cell aggravates diabetic nephropathy by disrupting PHB2 mediated mitophagy. *Redox Biol*. 2022;50:102260. https://doi.org/10.1016/j.redox.2022.102260
35. Staruschenko A, Spires D, Palygin O. Role of TRPC6 in progression of diabetic kidney disease. *Curr Hypertens Rep*. 2019;21:48. https://doi.org/10.1007/s11906-019-0960-9
36. Saqib U, Munjuluri S, Sarkar S, et al. Transient receptor potential canonical 6 (TRPC6) channel in the pathogenesis of diseases: a jack of many trades. *Inflammation*. 2023;46:1144–1160. https://doi.org/10.1007/s10753-023-01808-3
37. Ramirez GA, Coletto LA, Sciorati C, et al. Ion channels and transporters in inflammation: special focus on TRP channels and TRPC6. *Cells*. 2018;7:70. https://doi.org/10.3390/cells7070070

38. Hou X, Huang M, Zeng X, et al. The role of TRPC6 in renal ischemia/reperfusion and cellular hypoxia/reoxygenation injuries. *Front Mol Biosci*. 2021;8:698975. https://doi.org/10.3389/fmolb.2021.698975

39. Yi C, Wu W, Zheng D, et al. Targeted inhibition of endothelial calpain delays wound healing by reducing inflammation and angiogenesis. *Cell Death Dis*. 2020;11:533. https://doi.org/10.1038/s41419-020-02737-x

40. Davis MA, Fairgrieve MR, Den Hartigh A, et al. Calpain drives pyroptotic vimentin cleavage, intermediate filament loss, and cell rupture that mediates immunostimulation. *Proc Natl Acad Sci U S A*. 2019;116:5061–5070. https://doi.org/10.1073/pnas.1818598116

41. Jia SZ, Xu XW, Zhang ZH, et al. Selenoprotein K deficiency-induced apoptosis: a role for calpain and the ERS pathway. *Redox Biol*. 2021;47:102154. https://doi.org/10.1016/j.redox.2021.102154

42. Ong SB, Lee WH, Shao NY, et al. Calpain inhibition restores autophagy and prevents mitochondrial fragmentation in a human iPSC model of diabetic endotheliopathy. *Stem Cell Rep*. 2019;12:597–610. https://doi.org/10.1016/j.stemcr.2019.01.017

43. Liu X, Li M, Chen Z, et al. Mitochondrial calpain-1 activates NLRP3 inflammasome by cleaving ATP5A1 and inducing mitochondrial ROS in CVB3-induced myocarditis. *Basic Res Cardiol*. 2022;117:40. https://doi.org/10.1007/s00395-022-00948-1

44. Zhang M, Wang G, Peng T. Calpain-mediated mitochondrial damage: an emerging mechanism contributing to cardiac disease. *Cells*. 2021;10:2024. https://doi.org/10.3390/cells10082024

45. Chen Q, Thompson J, Hu Y, Dean J, Lesnefsky EJ. Inhibition of the ubiquitous calpains protects complex I activity and enables improved mitophagy in the heart following ischemia-reperfusion. *Am J Physiol Cell Physiol*. 2019;317:C910–C921. https://doi.org/10.1152/ajpcell.00190.2019

46. Guan L, Che Z, Meng X, et al. MCU Up-regulation contributes to myocardial ischemia-reperfusion Injury through calpain/OPA-1-mediated mitochondrial fusion/mitophagy Inhibition. *J Cell Mol Med*. 2019;23:7830–7843. https://doi.org/10.1111/jcmm.14662